Comparison of the dynamic response of one- and two-dimensional models for an embedded railway track to a moving load

M. Shamalta and A.V. Metrikine
Department of Civil Engineering and Geosciences, TU Delft, P.O. Box 5048, 2600 GA Delft, The Netherlands

In this paper, the steady-state response of an embedded track to the axle loading of a moving train is studied theoretically using two models. The first and the second models are one-dimensional (1D) and two-dimensional (2D), respectively, and differ by the fact that the latter model accounts for the lateral flexibility of the concrete slab of the track. The loading is modelled by a harmonically varying load that uniformly moves along the track. The response to this load is studied analytically with the help of the Fourier integral transforms. The study is accomplished performing the following steps, every of which is accompanied by comparison of two models under consideration. Firstly, the dispersion curves are calculated and critical parameters (frequency and velocity) of the load are found that could lead to resonance in the structure. Secondly, displacements of the rails and stresses in the concrete slab are studied for various velocities and frequencies of the load. The results obtained from both models are compared to that one calculated using a Finite Element program. On the basis of a comparative analysis of results obtained from the 1D and 2D models it is concluded that in engineering calculations, the 1D model can be employed for a quick and sufficiently accurate assessment of the dynamic behaviour of the embedded track under a high-speed train.

Keywords: Embedded railway track, high-speed train, moving load, dynamic response, radiation of elastic waves

1 Introduction

High-speed trains can be considered as one of the most impressive developments of modern civil engineering. As it happens with all revolutionary engineering developments, high-speed trains have brought a number of new problems railroad engineers have to deal with. These problems are mainly related to significant amplification of dynamic response of the railway track, which takes place when the train's speed approaches the velocity of surface (Rayleigh) waves in the track subsoil [1-11]. By moving with such a velocity the train can cause a pronounced amplification of the track response and generate powerful ground vibrations that can be perceptible at a large distance from the track. The Rayleigh-wave speed depends on the subsoil composition and can be in the range of 175-600 km/h. In soft (peat) subsoil, which is often met in The Netherlands, this velocity is in the order of 200 km/h and, consequently, can easily be exceeded by modern high-speed trains.

One of the most efficient ways to overcome the "soft soil problem" contains in introduction of a so-called "embedded" track. The structure of the embedded track that will be used in the Netherlands is shown in Fig. 1. Essentially, the structure is composed of a massive concrete slab into which the rails are embedded by means of Corkelast (Polyurethane mixed with Cork). This slab allows for efficient decoupling of the soil motion and the rail vibrations, thereby significantly reducing the impact of waves in the subsoil on the track dynamics.

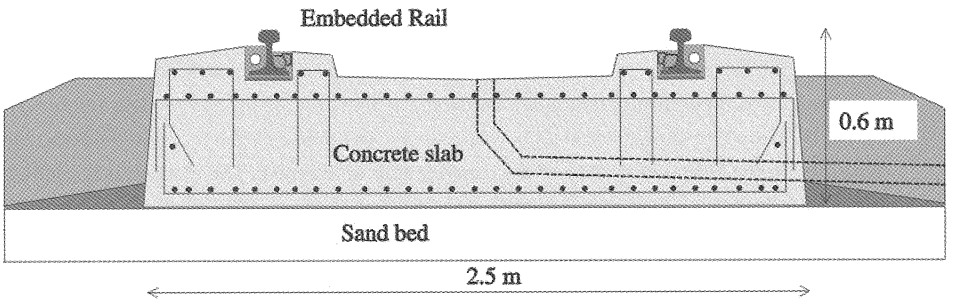

Fig. 1. Embedded railway structure

To design a new structure such as embedded track efficiently, it is useful to gain an insight into specific features of the dynamic behaviour of the structure. This can be done with the help of an analytical analysis of a simplistic model of the structure, which, however, takes into account main physical characteristics of the real structure at hand.

In this paper, we employ two models to investigate the dynamic response of the embedded track to the axle loading of a moving train. The first (simplified) model is one-dimensional and disregards the lateral flexibility of the slab. This model consists of two beams on elastic foundation, which are connected by continuous visco-elastic elements (fill material). The upper beam models the rails, whilst the lower one models the concrete slab. The foundation that supports the lower beam models the soil reaction.

The second model is two-dimensional and is composed of a plate on elastic foundation (slab on the ground), which interacts with two beams (rails) through continuous visco-elastic elements (fill material). Both models are subject to a moving harmonic load. In the first model, this load is applied to the upper beam. In the second model, both beams are loaded (not necessarily in-phase). The results obtained from both one-dimensional model and two-dimensional model are compared to that calculated using a finite element program "RAIL". This program has been developed in the faculty of Civil Engineering of Delft.

The aim of the paper is to compare the steady-state dynamic response of the aforementioned models of the embedded track and to determine the range of parameters in which the simplistic one-dimensional model is applicable.

2 Steady-state response of one-dimensional model

The one-dimensional (1D) model is presented in Fig. 2. This model is composed of two Euler-Bernoulli beams, a continuous visco-elastic element and a Winkler's foundation [13].

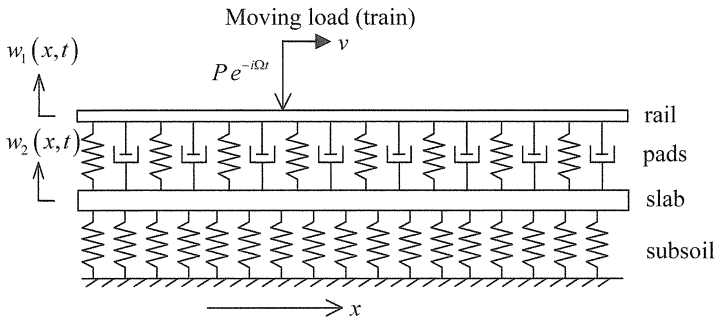

Fig 2. One-dimensional model for embedded railway track

The equations of motion describing the vertical forced vibrations of the beams read

$$\begin{aligned}
&\rho_1 A_1 \frac{\partial^2 w_1}{\partial t^2} + E_1 I_1 \frac{\partial^4 w_1}{\partial x^4} + k_d(w_1 - w_2) + c\left(\frac{\partial w_1}{\partial t} - \frac{\partial w_2}{\partial t}\right) = -Pe^{-i\Omega t}\delta(x - vt), \\
&\rho_2 A_2 \frac{\partial^2 w_2}{\partial t^2} + E_2 I_2 \frac{\partial^4 w_2}{\partial x^4} + k_d(w_2 - w_1) + c\left(\frac{\partial w_2}{\partial t} - \frac{\partial w_1}{\partial t}\right) + \chi w_2 = 0,
\end{aligned} \tag{1}$$

$$\lim_{|x-vt|\to\infty} \{w_1, w_2\} = 0 \tag{2}$$

In Eqs.(1)-(2), subscripts *i=1* and *i=2* are related to the upper beam (the rails) and the lower beam (the slab), respectively. Irrespective of the subscripts, $\omega_i(x,t)$ is the vertical displacement, ρ_i is the material density, A_i is the cross sectional area, E_i is the Young's modulus, I_i is the moments of inertia. Additionally, k_i and c are the stiffness and the damping constant of the material between the beams per unit length, χ is the stiffness of the foundation per unit length, P, Ω and v are the magnitude, angular frequency and velocity of the load, respectively.
The steady-state solution to Eqs. (1)-(2) can be derived by applying the following exponential Fourier transform over the time t:

$$w(x,t) = \frac{1}{2\pi}\int_{-\infty}^{\infty} \overline{w}(x,\omega)\,\exp(i\omega t)\,d\omega \quad \Leftrightarrow \quad \overline{w}(x,\omega) = \int_{-\infty}^{\infty} w(x,t)\,\exp(-i\omega t)\,dt. \tag{3}$$

Application of this transform to the system of differential equations (3) gives:

$$\begin{aligned}
&-\rho_1 A_1 \omega^2 \overline{w}_1 + E_1 I_1 \frac{\partial^4 \overline{w}_1}{\partial x^4} + k_d(\overline{w}_1 - \overline{w}_2) - i\omega c(\overline{w}_1 - \overline{w}_2) = \frac{P}{v}\exp\left(ix\frac{\omega - \Omega}{v}\right), \\
&-\rho_2 A_2 \omega^2 \overline{w}_2 + E_2 I_2 \frac{\partial^4 \overline{w}_2}{\partial x^4} + k_d(\overline{w}_2 - \overline{w}_1) - i\omega c(\overline{w}_2 - \overline{w}_1) + \chi \overline{w}_2 = 0.
\end{aligned} \tag{4}$$

The system of partial differential equations (1)-(2) has now been reduced to a system of ordinary differential equations (4).

The forced solution to equations (4), which describes the steady-state response of the system in the frequency domain, should be sought in the form

$$\begin{bmatrix} \overline{w}_1 \\ \overline{w}_2 \end{bmatrix} = \begin{bmatrix} c_1 \\ c_2 \end{bmatrix} \exp\left(ik_x x\right) \quad \text{with} \quad k_x = \frac{\omega - \Omega}{v} \tag{5}$$

Substitution of (5) into the system of equations (4) gives:

$$\begin{bmatrix} E_1 I_1 k_x^4 - \rho_1 A_1 \omega^2 + (k_d - i\omega c) & -(k_d - i\omega c) \\ -(k_d - i\omega c) & E_2 I_2 k_x^4 - \rho_2 A_2 \omega^2 + (k_d - i\omega c) + \chi \end{bmatrix} \begin{bmatrix} c_1 \\ c_2 \end{bmatrix} = \begin{bmatrix} P/v \\ 0 \end{bmatrix} \tag{6}$$

When solved with respect to c_1 and c_2, equation (6) yields:

$$\begin{cases} c_1 = P\left(E_2 I_2 k_x^4 - \rho_2 A_2 \omega^2 + (k_d - i\omega c) + \chi\right) / v / Q(\omega) \\ c_2 = P\left(k_d - i\omega c\right) / v / Q(\omega) \end{cases} \tag{7}$$

with

$$Q(\omega) = \left(E_1 I_1 k_x^4 - \rho_1 A_1 \omega^2 + k_d - i\omega c\right)\left(E_2 I_2 k_x^4 - \rho_2 A_2 \omega^2 + k_d - i\omega c + \chi\right) - \left(k_d - i\omega c\right)^2 . \tag{8}$$

Thus, the steady-state solution to the problem (1)-(2) is given as

$$w_{1,2}(x,t) = \frac{1}{2\pi} \exp\left(-ix\frac{\Omega}{v}\right) \int_{-\infty}^{\infty} c_{1,2}(\omega) \exp\left(i\omega\left(\frac{x}{v} - t\right)\right) d\omega . \tag{9}$$

The integral (9) can be evaluated by means of the contour integration. Since the integrand is a single-valued function, the result of integration is fully defined by the poles of this integrand. These poles are the roots of the denominator $Q(\omega)$ in expressions for $c_{1,2}(\omega)$, which is a polynomial of the order four with respect to the angular frequency ω. The poles can be found by a standard program for finding complex roots of a polynomial.

Denoting the poles that have a positive imaginary part as ω_k and the ones with a negative imaginary part as ω_m, and using the Jordan's lemma, the following expressions can be obtained for the displacement of the beams:

$$\begin{cases} w_1(x,t)\big|_{x>vt} = \dfrac{iP}{v} \exp\left(-ix\dfrac{\Omega}{v}\right) \displaystyle\sum_k \left\{ \frac{E_2 I_2 k_x^4 - \rho_2 A_2 \omega^2 + (k_d - i\omega c) + \chi}{\partial Q(\omega)/\partial\omega} \exp\left(i\omega\left(\frac{x}{v} - t\right)\right) \right\}_{\omega=\omega_k} \\ w_1(x,t)\big|_{x<vt} = -\dfrac{iP}{v} \exp\left(-ix\dfrac{\Omega}{v}\right) \displaystyle\sum_m \left\{ \frac{E_2 I_2 k_x^4 - \rho_2 A_2 \omega^2 + (k_d - i\omega c) + \chi}{\partial Q(\omega)/\partial\omega} \exp\left(i\omega\left(\frac{x}{v} - t\right)\right) \right\}_{\omega=\omega_m} \end{cases} \tag{10}$$

$$\begin{cases} w_2(x,t)\big|_{x>vt} = \dfrac{iP}{v} \exp\left(-ix\dfrac{\Omega}{v}\right) \displaystyle\sum_k \left\{ \frac{k_d - i\omega c}{\partial Q(\omega)/\partial\omega} \exp\left(i\omega\left(\frac{x}{v} - t\right)\right) \right\}_{\omega=\omega_k} \\ w_2(x,t)\big|_{x<vt} = -\dfrac{iP}{v} \exp\left(-ix\dfrac{\Omega}{v}\right) \displaystyle\sum_m \left\{ \frac{k_d - i\omega c}{\partial Q(\omega)/\partial\omega} \exp\left(i\omega\left(\frac{x}{v} - t\right)\right) \right\}_{\omega=\omega_m} \end{cases} \tag{11}$$

Before starting with numerical analysis of expressions (10)-(11), let us first consider the two-dimensional model and then analyse results of both models simultaneously, comparing them to each other.

3 Steady-state response of two-dimensional model

The two-dimensional (2D) model for an embedded railway track is shown in Fig. 3. The model consists of two Euler-Bernoulli beams, a Kirchhoff's plate, two continuous visco-elastic elements that connect the beams and the plate, a two-dimensional elastic foundation that is uniformly distributed beneath the plate and two uniformly moving harmonic loads.

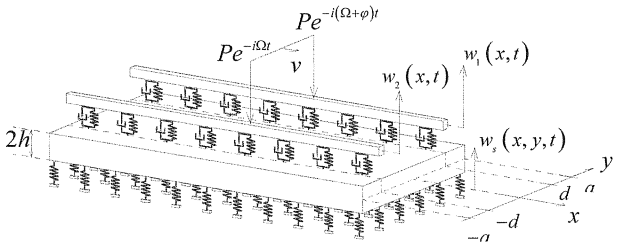

Fig. 3. Two-dimensional model for embedded railway track

Equations of motion governing the vertical forced vibrations of the beams and the plate can be written as [14,15]

$$\rho_r A_r \frac{\tilde{\partial}^2 w_1}{\partial t^2} + E_r I_r \frac{\tilde{\partial}^4 w_1}{\partial x^4} + k_d\left(w_1 - w_s(x,d,t)\right) + c\left(\frac{\tilde{\partial} w_1}{\partial t} - \frac{\tilde{\partial} w_s(x,d,t)}{\partial t}\right) = -P\exp\left(i(-\Omega t+\varphi)\right)\delta(x-vt), \tag{12}$$

$$\rho_r A_r \frac{\tilde{\partial}^2 w_2}{\partial t^2} + E_r I_r \frac{\tilde{\partial}^4 w_2}{\partial x^4} + k_d\left(w_2 - w_s(x,-d,t)\right) + c\left(\frac{\tilde{\partial} w_2}{\partial t} - \frac{\tilde{\partial} w_s(x,-d,t)}{\partial t}\right) = -P\exp\left(-i\Omega t\right)\delta(x-vt), \tag{13}$$

$$2\rho_s h \frac{\tilde{\partial}^2 w_s}{\partial t^2} + D\left(\frac{\tilde{\partial}^4 w_s}{\partial x^4} + 2\frac{\tilde{\partial}^4 w_s}{\partial x^2 \partial y^2} + \frac{\tilde{\partial}^4 w_s}{\partial y^4}\right) + \chi w_s + \left(k_d + c\frac{\tilde{\partial}}{\partial t}\right)\left(w_s - w_1\right)\delta(y-d) + \left(k_d + c\frac{\tilde{\partial}}{\partial t}\right)\left(w_s - w_2\right)\delta(y+d) = 0, \tag{14}$$

$$\left(\frac{\partial^2 w_s}{\partial y^2} + \upsilon\frac{\partial^2 w_s}{\partial x^2}\right)\Bigg|_{y=-a,a} = 0, \qquad \left(\frac{\partial^3 w_s}{\partial y^3} + (2-\upsilon)\frac{\partial^3 w_s}{\partial y \partial x^2}\right)\Bigg|_{y=-a,a} = 0, \tag{15}$$

$$\lim_{|x-vt|\to\infty}\left\{w_s, w_1, w_2\right\} = 0. \tag{16}$$

with $\omega_{1,2}(x,t)$ and $\omega_s(x,y,t)$ the vertical displacements of the rails and the concrete slab, respectively, ρ_r and ρ_s the material densities of the rails and the concrete slab, respectively, A_r the cross sectional area of the rail, $2h$ the thickness of the concrete slab, $2a$ the width of the plate, $2d$ the distance between rails, E_r and E_s the Young's modula of the rails and the concrete slab, respectively, $D=8E_sh^3/12/(1-\upsilon^2)$ the flexural rigidity of the plate (υ the Poisson's ratio of the concrete slab material), I_r the moment of inertia of the rail, k_d and c the stiffness and the damping constant of the fill material per unit length, respectively, χ the stiffness of the elastic foundation per unit area, P the magnitude of the loads, Ω the angular frequency of the loads, v the velocity of the loads and φ the phase shift between vibrations of the loads. The symbols $\tilde{\partial}$ and ∂ denote the generalised and classical derivatives, respectively, see [16].

Equations (12) and (13) describe the dynamic equilibrium of vertical vibrations of a differential element of the beams. Equation (14) gives the dynamic equilibrium of vertical vibrations of the plate. Equations (15) show that neither bending moment nor vertical force is applied to the edges of the plate. Equation (16) presents the requirement that at infinite distance from the moving load the steady-state vibrations of the structure must vanish.
To find the steady-state response of the system, the following integral Fourier transforms over the time and co-ordinate are applied:

$$\begin{aligned}
\overline{w}_s(k_x,y,\omega)&=\int_{-\infty}^{\infty}\int_{-\infty}^{\infty} w_s(x,y,t)\,\mathrm{e}^{i(\omega t-k_x x)}dxdt \quad\Leftrightarrow\quad w_s(x,y,t)=\frac{1}{(2\pi)^2}\int_{-\infty}^{\infty}\int_{-\infty}^{\infty}\overline{w}_s(k_x,y,\omega)\mathrm{e}^{-i(\omega t-k_x x)}dk_x d\omega,\\
\overline{w}_{1,2}(k_x,\omega)&=\int_{-\infty}^{\infty}\int_{-\infty}^{\infty} w_{1,2}(x,t)\,\mathrm{e}^{i(\omega t-k_x x)}dxdt \quad\Leftrightarrow\quad w_{1,2}(x,t)=\frac{1}{(2\pi)^2}\int_{-\infty}^{\infty}\int_{-\infty}^{\infty}\overline{w}_{1,2}(k_x,\omega)\mathrm{e}^{-i(\omega t-k_x x)}dk_x d\omega.
\end{aligned} \tag{17}$$

Application of these transforms to the governing equations (12)-(16) yields

$$\begin{aligned}
&(-\rho_r A_r\omega^2+E_r I_r k_x^4+k_d-ic\omega)\overline{w}_1(k_x,\omega)-(k_d-ic\omega)\overline{w}_s(k_x,d,\omega)\\
&\qquad=-2\pi P e^{i\varphi}\delta(\omega-k_x v-\Omega),
\end{aligned} \tag{18}$$

$$\begin{aligned}
&(-\rho_r A_r\omega^2+E_r I_r k_x^4+k_d-ic\omega)\overline{w}_2(k_x,\omega)-(k_d-ic\omega)\overline{w}_s(k_x,-d,\omega)\\
&\qquad=-2\pi P\delta(\omega-k_x v-\Omega),
\end{aligned} \tag{19}$$

$$\begin{aligned}
&D\frac{\tilde{\partial}^4\overline{w}_s(k_x,y,\omega)}{\partial y^4}-2Dk_x^2\frac{\tilde{\partial}^2\overline{w}_s(k_x,y,\omega)}{\partial y^2}+(-2\rho_s h\omega^2+Dk_x^4+\chi)\overline{w}_s(k_x,y,\omega)=\\
&\qquad-(k_d-i\omega c)\left((\overline{w}_s-\overline{w}_1)\delta(y-d)+(\overline{w}_s-\overline{w}_2)\delta(y+d)\right),
\end{aligned} \tag{20}$$

$$\left(\frac{\partial^2\overline{w}_s}{\partial y^2}-\upsilon k_x^2\overline{w}_s\right)\Bigg|_{y=\pm a}=0, \qquad \left(\frac{\partial^3\overline{w}_s}{\partial y^3}-(2-\upsilon)k_x^2\frac{\partial\overline{w}_s}{\partial y}\right)\Bigg|_{y=\pm a}=0 \tag{21}$$

Equation (20) is a linear differential equation that contains generalised derivatives. At this stage of analysis, it is customary to replace this equation by a system of equations that employ the classical derivatives only. To this end, the relations between the classical and generalised derivatives are to be applied (as shown in Appendix A) to give

$$D\frac{\partial^4 \overline{w}_s}{\partial y^4} - 2Dk_x^2 \frac{\partial^2 \overline{w}_s}{\partial y^2} + (-2\rho_s h\omega^2 + Dk_x^4 + \chi)\overline{w}_s = 0, \tag{22}$$

$$\overline{w}_s\big|_{y=\pm d+0} = \overline{w}_s\big|_{y=\pm d-0}, \quad \left.\frac{\partial \overline{w}_s}{\partial y}\right|_{y=\pm d+0} = \left.\frac{\partial \overline{w}_s}{\partial y}\right|_{y=\pm d-0}, \quad \left.\frac{\partial^2 \overline{w}_s}{\partial y^2}\right|_{y=\pm d+0} = \left.\frac{\partial^2 \overline{w}_s}{\partial y^2}\right|_{y=\pm d-0}, \tag{23}$$

$$\left.\frac{\partial^3 \overline{w}_s}{\partial y^3}\right|_{y=+d+0} - \left.\frac{\partial^3 \overline{w}_s}{\partial y^3}\right|_{y=+d-0} = -\frac{k_d - i\omega c}{D}\left(\overline{w}_s\big|_{y=d} - \overline{w}_1\right), \quad \left.\frac{\partial^3 \overline{w}_s}{\partial y^3}\right|_{y=-d+0} - \left.\frac{\partial^3 \overline{w}_s}{\partial y^3}\right|_{y=-d-0} = -\frac{k_d - i\omega c}{D}\left(\overline{w}_s\big|_{y=-d} - \overline{w}_2\right). \tag{24}$$

Equation (22) describes the plate motion everywhere but not along the lines $y=\pm d$. These lines are accounted for in the boundary conditions (23) and (24) that describe the continuity of the displacement, slope and curvature of the plate and the balance of vertical forces between the plate and the visco-elastic elements at $y=\pm d$, respectively.
The general solution to equation (22) reads

$$\overline{w}_s(k_x, y, \omega) = \sum_{n=1}^{4} A_n e^{\lambda_n y}. \tag{25}$$

with the roots of the following equation

$$\lambda_n^4 - 2k_x^2\lambda_n^2 + \left(\frac{\chi - 2\rho_s h\omega^2}{D} + k_x^4\right) = 0, \tag{26}$$

which are given as

$$\lambda_1 = \sqrt{k_x^2 + \sqrt{\frac{2\rho_s h\omega^2 - \chi}{D}}}, \quad \lambda_2 = \sqrt{k_x^2 - \sqrt{\frac{2\rho_s h\omega^2 - \chi}{D}}}, \quad \lambda_3 = -\lambda_1, \quad \lambda_4 = -\lambda_2. \tag{27}$$

Employing now the general solution given by Eq. (25), using Eqs. (27), and taking into account that there are three homogeneous parts of the plate ($-a \le y \le -d$, $|y| \le d$ *and* $d \le y \le a$), the Fourier-displacement of the plate can be expressed as

$$\overline{w}_s(k_x, y, \omega) = A_{j+1}(k_x, \omega)e^{\lambda_1 y} + A_{j+2}(k_x, \omega)e^{\lambda_2 y} + A_{j+3}(k_x, \omega)e^{-\lambda_1 y} + A_{j+4}(k_x, \omega)e^{-\lambda_2 y} \tag{28}$$

with

$$j = \begin{cases} 0 & -a \le y \le -d \\ 4 & -d \le y \le +d \\ 8 & +d \le y \le +a \end{cases}.$$

Substitution of Eq. (28) into the equations for the rail vibrations (18) and (19), into the boundary conditions at the edges of the plate (21) and at the interface conditions along the lines $y=\pm d$ (23) and (24), results in a system of twelve linear algebraic equations with respect to A_1-A_{12}. This system of equations can be written as follows

$$a_{ij} \cdot A_j = F_i \cdot \delta(k_x v + \omega - \Omega), \; i = 1..12, \; j = 1..12, \tag{29}$$

with a_{ij} and F_i defined in Appendix C. Unknown coefficients A_1-A_{12} can be found from Eq.(29) with the help of a standard program for solution of a system of linear algebraic equations with complex coefficients.

Considering A_1-A_{12} as known, final expressions for the displacements of the plate and the beams in the space-time domain can be obtained by applying the inverse Fourier transforms defined by (17) to Eqs. (28), (18) and (19) (into the latter equations, equation (28) has to be first substituted). This yields

$$w_s(x,y,t) = \frac{\exp(-i\Omega t)}{(2\pi)^2} \int_{-\infty}^{\infty} Q_s(k_x, y) \exp(i(x - vt)k_x)\, dk_x , \tag{30}$$

$$w_1(x,t) = \frac{\exp(-i\Omega t)}{(2\pi)^2} \int_{-\infty}^{\infty} \left(\frac{(k_d - ic\omega) Q_s(k_x, d) k_d - 2\pi P \exp(i\varphi)}{-\rho_r A_r \omega^2 + E_r I_r k_x^4 + k_d - ic\omega} \right) \exp(i(x - vt)k_x)\, dk_x , \tag{31}$$

$$w_2(x,t) = \frac{\exp(-i\Omega t)}{(2\pi)^2} \int_{-\infty}^{\infty} \left(\frac{(k_d - ic\omega) Q_s(k_x, -d) k_d - 2\pi P}{-\rho_r A_r \omega^2 + E_r I_r k_x^4 + k_d - ic\omega} \right) \exp(i(x - vt)k_x)\, dk_x , \tag{32}$$

with

$$Q_s(k_x, y) = A_{j+1}(k_x, \omega) e^{+\lambda_1 y} + A_{j+2}(k_x, \omega) e^{+\lambda_2 y} + A_{j+3}(k_x, \omega) e^{-\lambda_1 y} + A_{j+4}(k_x, \omega) e^{-\lambda_2 y}$$

and

$$\omega = \Omega + k_x v .$$

Equation (33) plays a fundamental role in the steady-state response of elastic structures to moving loads. This equation relates the frequencies and wavenumbers of the waves that are perturbed in the structure (in the steady-state regime) to the kinematic characteristics of the loads and. Because Eq.(33) is independent of the wave amplitude and the load's amplitude, and only relates their kinematic characteristics, this equation is referred to as a *kinematic invariant*. For the first time, this invariant has been elaborated by Vesnitskii [17] and has been employed later in a number of studies, see [5, 18, 19]. Physically, the kinematic invariant provides a necessary condition for waves to be generated by the loads in a resonance manner.

4 Dispersion analysis

Before starting with analysis of the structural response to the moving loads, it is worth discussing the dispersion of waves that may propagate along the structure (in the x-direction). The wavenumber k_x and the radial frequency ω of these waves are to be found from the dispersion relation, which is given for the 1D model as

$$Q(\omega) = 0 , \tag{34}$$

and for the 2D model as

$$\det[a] = 0 \tag{35}$$

with $Q(\omega)$ defined by Eq. (8) and matrix $[a]$ presented in Appendix C. To find real pairs of k_x and ω that satisfy the dispersion equations (34) and (35), the damping c in the fill material has to be turned to zero.

In Fig. 4 the dispersion curves, which visualise the real pairs of ω and k_x turning Eqs. (34) and (35) to zero are depicted for both models. Hereinafter, physical parameters of both 1D and 2D structures are used, which are given in Appendix B. The dashed-pointed curves in this figure are dispersion curves for the 1D model, whereas the solid and dashed curves correspond to the 2D model. The reason to use two different lines for the 2D model is that waves, which propagate along the structure, can be either symmetric (solid lines) or antisymmetric (dashed lines) with respect to the centre line of the plate.

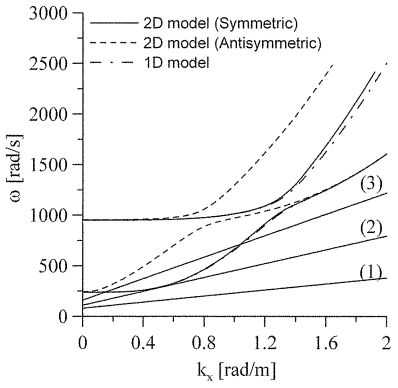

Fig. 4. Dispersion curves and the kinematic invariant

The main difference between the dispersion curves of the models is that the 1D model possesses just two dispersion curves, while the two-dimensional model has infinitely many curves because of infinite number of normal modes that may be excited in the plate in the lateral direction. Fig. 4 shows only the first four dispersion curves for the 2D model since the higher modes are of no significance for the system response. One can see from Fig. 4 that the lowest dispersion curve of the 1D model approximates the lowest dispersion curve (the first symmetric mode) of the 2D model very well. Further, the second curve of the 1D model almost perfectly coincides with the second symmetric mode of the 2D model.

The partial agreement between the dispersion curves in the "low-frequency" range gives a hope that for relatively "small" velocities and frequencies of the load the structural responses predicted by the models may be close.

Using the dispersion curves the frequencies and wavenumbers of the waves that the load perturbs in the structures can be found geometrically. To this end the kinematic invariant $\omega = k_x v + \Omega$ (see Eqs. (5) or (33)) has to be plotted in the dispersion plane as depicted in Fig. 4. By doing so, one can distinguish three cases. First, the kinematic parameters v and Ω of the loads are such that the kine-

matic invariant has no crossing points with the dispersion curves (straight line "1" in Fig. 4). In this case, which is referred to as the *sub-critical motion*, the load does not radiate waves (that could propagate towards infinity in the undamped structure) and the displacement field perturbed by the loads in the beams and the plate is localised in the vicinity of the loads (exponentially decays with the distance from the loads). Secondly, the kinematic parameters of the loads parameters are such that the kinematic invariant has crossing points with the dispersion curves (straight line "3"). In this case, which is referred to as the *super-critical motion*, the loads generate waves, which propagate along the structure with a constant amplitude (in the undamped case). These waves transfer energy from the loads with a velocity equal to their group velocity v_{gr}. In accordance with the radiation condition [17, 20], waves must carry out energy away from the loads. This means that a wave, with a group velocity larger than the velocity of the loads, i.e. $v_{gr}>v$, must propagate in front of the loads, whereas a wave with $v_{gr}<v$ must propagate behind the loads. Thirdly, v and Ω are such that the kinematic invariant is tangential to one of the dispersion curves (straight line "2"). In this case, which is referred to as the *critical motion*, the group velocity of the radiated into the structure waves is equal to the velocity of the loads, $v_{gr} = v$. This implies that the energy is not transported away from the loads but is accumulated in their vicinity, leading to amplification of the system response, i.e. to resonance. The pairs of v and Ω that lead to resonance for 2D and 1D models are shown in Figures 5a and 5b, respectively. In Fig. 5a the solid and dashed lines represent the resonance pairs for the symmetric and antisymmetric loading, respectively. We will call the curves, which are shown in Fig. 5, as *bifurcation curves* because these curves not only show the resonance load parameters but also break the (Ω,v)-plane into domains that correspond to qualitatively different structural response. For example, considering the 2D model, one can say that the loads with parameters form domain "I" can not generate propagating waves in the structures. Domain "II", being separated from domain "I" by a solid line, allows for radiation of two symmetric waves in the structure. Passing to domain "III" through a dashed line introduces a possibility of having two antisymmetric waves in addition to the two symmetric ones, etc.

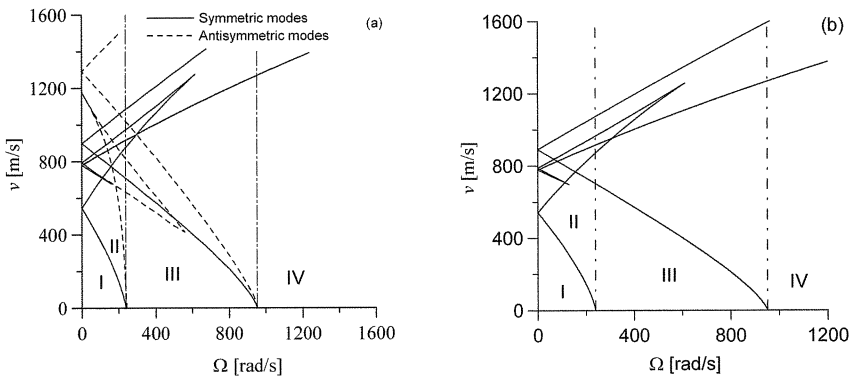

Fig. 5. Bifurcation curves

As Fig. 5 shows, there are many (for the 2D model, infinitely many) possibilities for waves to be generated by the loads. These possibilities are concerned with the distribution of waves in front

and behind the load, with the number of radiated waves and, for the two-dimensional model, with the mode of the plate vibrations that accompanies waves propagating along the structure. Comparing Figures 5a and 5b, one can see that the bifurcation curves of the 1D model partly reflect those of the 2D model. More precisely, as the dispersion curves (Fig. 4) show, the 1D model predicts bifurcations that are related to the first two symmetric modes of the 2D model. To find it out, whether the other modes of the 2D model have a perceptible impact on the structural response, in the next section the displacement patterns in both structures are studied for the load parameters, which belong to domains I and III in Fig. 5. These domains are chosen since they correspond to velocities that are achievable for modern high-speed trains.

5 Comparison of displacements

The displacements of the structures are calculated numerically by evaluating the integrals given by Eqs. (10)-(11) and Eqs. (30)-(32). The displacement patterns of the rails resulting from both models are presented in Figures 6-7 for the time moment $t=0$ and the parameters presented in appendix B. In Figures 6a and 7a the displacements resulting from the models are compared for the in-phase ($\varphi=0$) loading of the 2D model, whilst in Figures 6b and 7b the comparison is shown for the anti-phase ($\varphi=\pi$) loading.

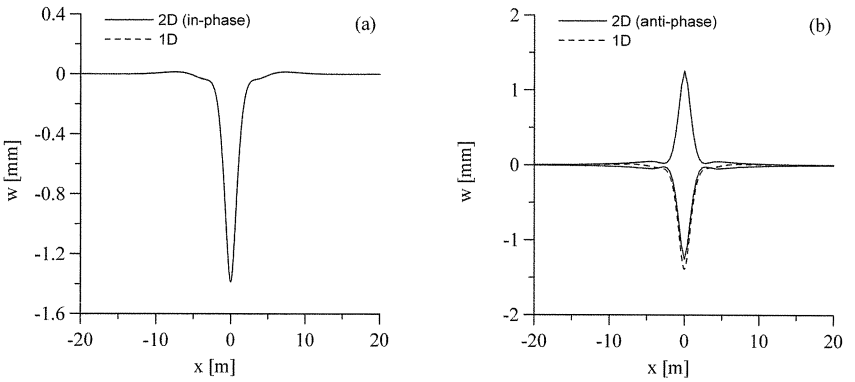

Fig. 6. Displacement of the rails for $\Omega=100$ rad/s, $v=100$ m/s (domain I)

Fig. 6 corresponds to domain I in Fig. 5 ($\Omega=100$ rad/s, $v=100$ m/s). In accordance with the dispersion analysis, the loads, having parameters from this domain, do not perturb propagating waves in the structure (the kinematic invariant does not cross the dispersion curves). Consequently, the displacement patterns, which are shown in Fig. 6, are localised in the vicinity of the loads.
Fig. 6a shows that in the case of the in-phase loading, the response of both models is almost exactly the same. This is to be expected since the lowest dispersion curves of both models are almost exactly the same. Fig. 6b presents a less expectable result, namely that even in the case of the anti-phase loading of the 2D model, its response can be quite well predicted by the 1D model. This implies that for the parameters under consideration the left and the right halves of the 2D model (with respect to the centreline of the plate) respond almost independently.
Fig. 7 corresponds to the loading with parameters form domain III. In accordance with the kine-

matic analysis, this domain allows for two waves in the 1D model and for two symmetric and two antisymmetric waves in the 2D model to be generated by the load.

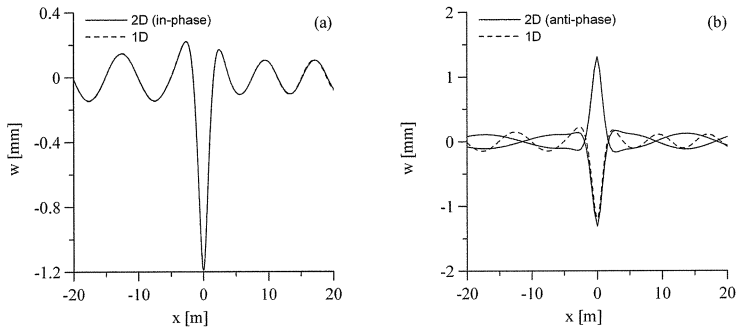

Fig. 7. Displacement of the rails and the slab for Ω=400 rad/s, v =100 m/s (domain III)

The in-phase loading of the 2D model can perturb only two symmetric waves. These waves are clearly seen in Fig. 7a. The wave propagating in front of the load is shorter than that propagating behind the load, which is in correspondence with the Doppler effect. Likewise in the previous case, the response of the 1D model very well resembles that of the 2D model (being loaded in-phase). This resemblance worsens in the case of the anti-phase loading as it can be seen from Fig. 7b. This, however, is to be expected, since the 1D model is not able to describe asymmetric waves in the slab. Proceeding towards higher (with respect to the load velocity) domains in Fig. 5, would complicate the response pattern, because of a larger number of waves perturbed by the loads. Furthermore, results of the two models will deviate more and more. Performing such analysis, however, seems to be irrelevant because the higher velocities are not reachable for modern high-speed trains.

Finalising this section, it is worth showing the maximum displacement of the rails that occurs under various parameters of the loads. The maximum displacement is calculated over the period of the load vibration and considering a sufficient length of the rails around the loading points. For the 2D model, both the in-phase and anti-phase loading are taken into account.

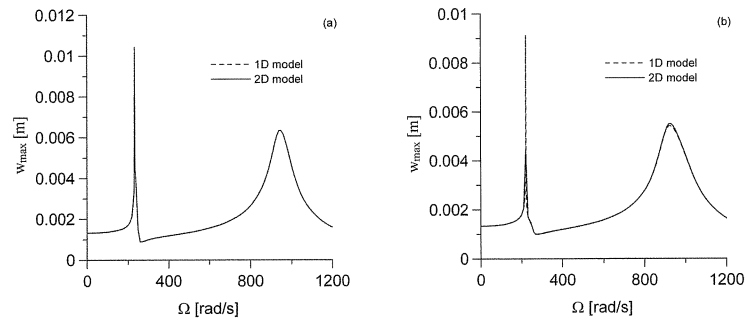

Fig. 8. Maximum displacement of the rails versus frequency of the load for a) v=30 m/s and b) v=80 m/s

The maximum displacement is depicted in Fig. 8 versus the angular frequency of the load for two load's velocities.

This figure shows that the models predict almost the same maximum displacement so that the much simpler 1D model is capable of predicting the maximum possible displacement of an embedded track at velocities that are realistic for modern high-speed trains.

It is important to note that the maximum displacement grows significantly at certain frequencies of the load, which correspond to the bifurcation curves that are shown in Fig. 5. Thus, Fig. 8 confirms that bifurcation curves predict resonance amplification of the structural response.

6 Comparison of stresses in the concrete slab

It is of practical importance to know the dynamic stress distribution in the concrete slab. In the frame of the 2D model, this distribution can be found on the basis of Eq.(30) by employing the following expressions for the stresses in the Kirchhoff's plate:

$$\sigma_{xx} = -\frac{3D}{2h^2}\left(\frac{\partial^2 w}{\partial x^2} + \nu\frac{\partial^2 w}{\partial y^2}\right),\ \sigma_{yy} = -\frac{3D}{2h^2}\left(\nu\frac{\partial^2 w}{\partial x^2} + \frac{\partial^2 w}{\partial y^2}\right),\ \sigma_{xy} = -\frac{3D(1-\nu)}{2h^2}\frac{\partial^2 w}{\partial x \partial y} \tag{36}$$

Substitution of the expression for the plate displacement (30) into Eqs.(36) yields:

$$\sigma_{xx}(x,y,t) = \frac{3D\exp(-i\Omega t)}{2h^2(2\pi)^2}\int_{-\infty}^{\infty} Q_{xx}(k_x,y)\exp\left(i(x-vt)k_x\right)dk_x \tag{37}$$

$$\sigma_{yy}(x,y,t) = \frac{3D\exp(-i\Omega t)}{2h^2(2\pi)^2}\int_{-\infty}^{\infty} Q_{yy}(k_x,y)\exp\left(i(x-vt)k_x\right)dk_x \tag{38}$$

$$\sigma_{xy}(x,y,t) = \frac{-3Di(1-\nu)\exp(-i\Omega t)}{2h^2(2\pi)^2}\int_{-\infty}^{\infty} k_x Q_{xy}(k_x,y)\exp\left(i(x-vt)k_x\right)dk_x \tag{39}$$

with

$$\begin{aligned} Q_{xx}(k_x,y) = {} & A_{j+1}(k_x,\omega)\times(k_x^2-\nu\lambda_1^2)e^{+\lambda_1 y} + A_{j+2}(k_x,\omega)\times(k_x^2-\nu\lambda_2^2)e^{+\lambda_2 y} \\ & + A_{j+3}(k_x,\omega)\times(k_x^2-\nu\lambda_1^2)e^{-\lambda_1 y} + A_{j+4}(k_x,\omega)\times(k_x^2-\nu\lambda_2^2)e^{-\lambda_2 y}, \end{aligned}$$

$$\begin{aligned} Q_{yy}(k_x,y) = {} & A_{j+1}(k_x,\omega)\times(\nu k_x^2-\lambda_1^2)e^{+\lambda_1 y} + A_{j+2}(k_x,\omega)\times(\nu k_x^2-\lambda_2^2)e^{+\lambda_2 y} \\ & + A_{j+3}(k_x,\omega)\times(\nu k_x^2-\lambda_1^2)e^{-\lambda_1 y} + A_{j+4}(k_x,\omega)\times(\nu k_x^2-\lambda_2^2)e^{-\lambda_2 y}, \end{aligned}$$

$$\begin{aligned} Q_{xy}(k_x,y) = {} & A_{j+1}(k_x,\omega)\times\lambda_1 e^{+\lambda_1 y} + A_{j+2}(k_x,\omega)\times\lambda_2 e^{+\lambda_2 y} \\ & - A_{j+3}(k_x,\omega)\times\lambda_1 e^{-\lambda_1 y} - A_{j+4}(k_x,\omega)\times\lambda_2 e^{-\lambda_2 y}. \end{aligned}$$

Expressions (37)-(39) show that the dynamic stresses in the plate depend on the frequency and velocity of the loads. This dependence is similar to that of the plate's displacement in the sense that it is determined by the domain in the bifurcation plane (Fig. 5) to which the parameters of the loads

belong. To demonstrate this, in Figures 9 and 10 the distribution of stresses σ_{xx} in the plate is plotted for the parameters of the load belonging to domains I and III in the bifurcation plane (Fig. 5). Fig. 9 shows the stress distribution at $t=0$ for Ω=100 rad/s and v=100 rad/s, that is for the load parameters belonging to domain I (no wave radiation). Fig. 10 corresponds to domain III (two symmetric and two antisymmetric waves can be generated) of the bifurcation plane, presenting the stress distribution for Ω=400 rad/s and v=100 rad/s. Fig. 10a shows the stress under the in-phase loading, whereas Fig. 10b presents that under the anti-phase loading.

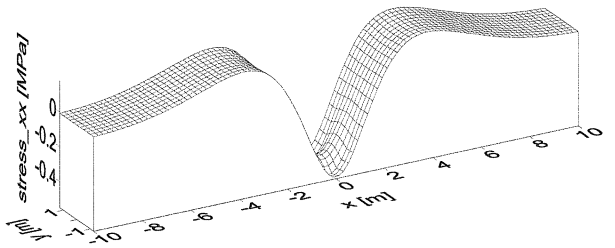

Fig. 9. Distribution of the stress σ_{xx} in the concrete slab for (Ω,v)=(100 rad/s, 100 m/s)

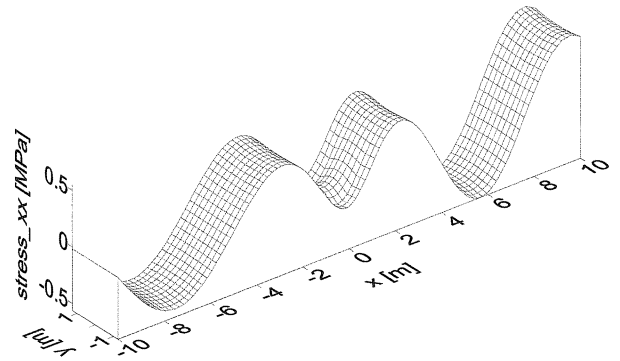

Fig. 10a. Distribution of the stress σ_{xx} in the concrete slab for (Ω,v)=(400 rad/s, 100 m/s) under in-phase loading

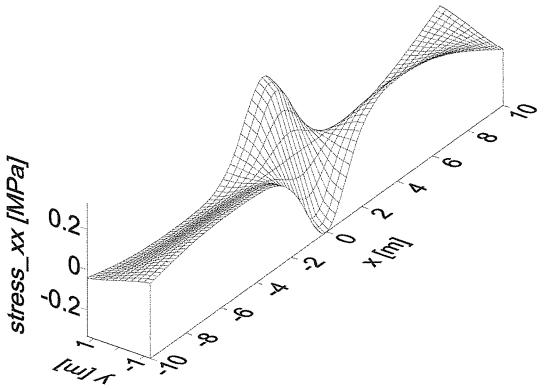

Fig. 10b. Distribution of the stress σ_{xx} in the concrete slab for (Ω,v)=(400 rad/s, 100 m/s) under anti-phase loading

Fig. 9 shows that in the sub-critical motion of the load, the stresses in the plate are exponentially localised in the vicinity of the load and the maximum stress takes place right beneath the loading points. In the sub-critical motion, as it can be seen from Fig. 10, the situation changes. In correspondence with the dispersion analysis, the loads generate waves in the slab. Accordingly, the maximum stress does not necessarily takes place under the loads but may occur at a certain distance from them, likewise in the case of the in-phase loading depicted in Fig. 10a.

Let us calculate the maximum values of the stresses σ_{xx}, σ_{xy} and σ_{yy} that occur in the plate under given loading parameters (the maximum is taken over the period of the load's vibration and by taking into account a sufficient area of the plate around the load). The maximum stresses are shown in Fig. 11a versus the angular frequency of the load for the load's velocity v=80 m/s. This figure shows that the stress σ_{xx} that occurs under the in-phase loading, is the largest for almost all frequencies of the load. Therefore, to assess the upper limit of the stress in the concrete slab, it is sufficient to analyse only this (σ_{xx}) component of the stress tensor. If this is so, then it is natural to pose the following question: could not we use the simple 1D model to calculate this stress with an acceptable accuracy? To answer this question, let us compare σ_{xx} as it results from the 1D and 2D models.

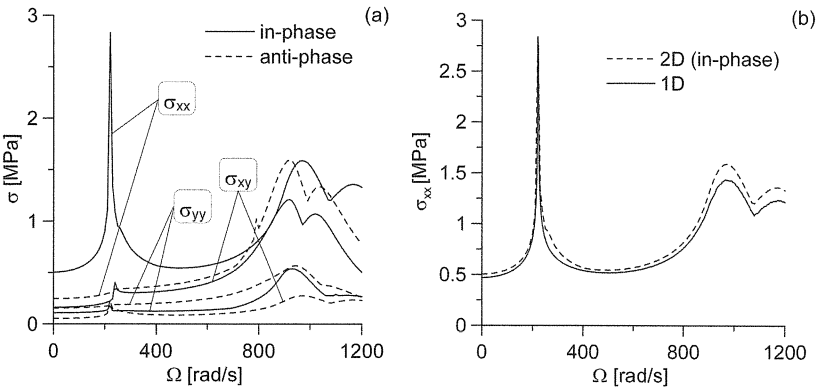

Fig. 11. Maximum stresses in the concrete slab versus the frequency of the load for v=80 m/s

To calculate the x-component of the stress in the slab in the frame of the 1D model, the following expression should be used (with notations used in Eq.(1)):

$$\sigma_{xx} = -\frac{hE_2}{2}\frac{d^2 w_2}{dx^2}. \tag{40}$$

The maximum stress σ_{xx} as it results from the 1D model (Eq.(40)) and 2D model (Eq.(37)) is shown in Fig. 11b as a function of the load's frequency for v=80 m/s. This figure shows a very good resemblance of the predictions of the 1D and 2D models. This allows us to conclude that the 1D model can be used for a quick and reasonably accurate assessment of the maximum stress in the concrete slab.

7 Conclusions

The steady-state response of an embedded track to the axle loading of a moving train has been studied theoretically using two models. The first model is one-dimensional (1D) and neglects the lateral flexibility of the concrete slab of the track. This model consists of two Euler-Bernoulli beams connected by a continuous visco-elastic element and supported by the Winkler's foundation. The upper and the lower beams represent the rails and the concrete slab, respectively. The visco-elastic element is employed to model the fill material (Corkelast) that is placed between the rails and the concrete slab. The foundation represents the soil's reaction. The second model is two-dimensional (2D) and, therefore accounts for the lateral flexibility of the concrete slab. This model consists of two beams (rails) and a flexible plate (slab), which interacts with the beams through continuous visco-elastic elements (fill material). The plate is supported by a two-dimensional elastic foundation of the Winkler's type.

A study of wave propagation in both structures has been accomplished followed by the kinematic analysis of waves, which can be generated by the axle loading, which is modelled with the help of a harmonically varying load that uniformly moves along the rails. In the course of this study, it has been found that the one-dimensional model possesses two dispersion curves, which correspond to flexural waves that may propagate in two beams, which compose the model. The two dimensional model, on the contrary, possesses an infinite number of dispersion curves, each pair of which corresponds to a lateral mode of vibrations of the plate. Despite this apparent difference, the dispersion curves of the 1D model very well approximate two dispersion branches of the 2D model that correspond to the two lowest symmetric modes of the plate vibrations.

Bifurcation pairs of the load's frequency and load's velocity (critical velocities) have been found, which lead to resonance in the structure. These pairs are plotted in the plane "load velocity – load frequency" in the form of *bifurcation curves*. If the load parameters belong to one of these curves, then resonance response of the structure should be expected. Additionally, the bifurcation curves break the plane into domains that correspond to different wave patterns to be generated by the load.

The vertical displacement of the rails has been calculated and analysed in the frame of both models for various velocities and frequencies of the load. The analysis has shown that the 1D model is capable of quite an accurate prediction of the rail's displacement.

The maximum (over time and space) displacement of the rails has been studied as a function of the load's frequency for two specific velocities of the load. It has been shown that resonance picks of this function exactly correspond to the load parameters predicted by the bifurcation curves.

Analytical results obtained from both one-dimensional model and two-dimensional model have been compared to that calculated using a finite element program "RAIL". It has been shown that there is a good agreement between the results.

The stresses and their maximum values in the concrete slab have been calculated and analysed using the 2D model for various velocities and frequencies of the load. Analysing the maximum stresses, it has been shown that the stress in the Ω-direction that occurs under the in-phase loading of the structure is the largest one and therefore can be used for assessment of the maximum possible stress in the plate. Comparing this stress as it results from the 1D and 2D models (the former is also capable of predicting this stress), it has been found that the 1D model predicts the stress with quite a high accuracy.

Thus, on the basis of analysis that has been carried out in this paper, it can be concluded that in engineering calculations, the one-dimensional model can be employed for a quick and sufficiently accurate assessment of the dynamic behaviour of the embedded track.

Finalising the paper, we ought to mention the weakest point of the models that have been considered. This point is concerned with the modelling of the soil reaction. In this paper, it has been done with the help of elastic foundation of the Winkler's type. Such a modelling is approximate, for the soil equivalent stiffness, as it has been shown in [21], is a complex function that depends on the frequency and wavelength of the wave process, which takes place in the concrete slab. The reason to replace this complicated soil reaction by the simplistic Winkler's foundation, which takes into account the static component of the soil reaction only, is that the slab is very stiff and, therefore, one might expect that the dynamic coupling between the track and the subsoil is very small. This expectation, however, has to be proven by incorporating into the model a proper soil-slab dynamic coupling.

Appendix A

The generalised derivatives are applied to the functions that are discontinuous or have discontinues derivatives [16]. In equation (20) the discontinuity takes place along the straight lines $y=\pm d$. In accordance with the general definition [16], the generalised and classical derivatives at $y=\pm d$ are related as follows:

$$\frac{\tilde{\partial} w}{\partial y}=\frac{\partial w}{\partial y}+[w]_{y=\pm d}\,\delta(y\mp d), \tag{A41}$$

$$\frac{\tilde{\partial}^2 w}{\partial y^2}=\frac{\partial^2 w}{\partial y^2}+\left[\frac{\partial w}{\partial y}\right]_{y=\pm d}\delta(y\mp d)+[w]_{y=\pm d}\frac{d}{dy}\delta(y\mp d), \tag{A42}$$

$$\frac{\tilde{\partial}^3 w}{\partial y^3}=\frac{\partial^3 w}{\partial y^3}+\left[\frac{\partial^2 w}{\partial y^2}\right]_{y=\pm d}\delta(y\mp d)+\left[\frac{\partial w}{\partial y}\right]_{y=\pm d}\frac{d}{dy}\delta(y\mp d)+[w]_{y=\pm d}\frac{d^2}{dy^2}\delta(y\mp d), \tag{A43}$$

$$\frac{\tilde{\partial}^4 w}{\partial y^4}=\frac{\partial^4 w}{\partial y^4}+\left[\frac{\partial^3 w}{\partial y^3}\right]_{y=\pm d}\delta(y\mp d)+\left[\frac{\partial^2 w}{\partial y^2}\right]_{y=\pm d}\frac{d}{dy}\delta(y\mp d)+\left[\frac{\partial w}{\partial y}\right]_{y=\pm d}\frac{d^2}{dy^2}\delta(y\mp d)+[w]_{y=\pm d}\frac{d^3}{dy^3}\delta(y\mp d), \tag{A44}$$

with and denoting the generalised derivative and the classical derivative, respectively, and the square brackets defining the jump of the in-bracket function at the discontinuity, for example $[\omega(y)]_{y=\pm d} = \omega(\pm d+0)-\omega(\pm d-0)$.

Substituting equations (A41)-(A44) into equation (20) and separating the terms that are multiplied by different derivatives of the delta function, we obtain the following system of equations:

$$D\frac{\partial^4 \overline{w}_s}{\partial y^4} - 2Dk_x^2 \frac{\partial^2 \overline{w}_s}{\partial y^2} + (-2\rho_s h\omega^2 + Dk_x^4 + \chi)\overline{w}_s = 0, \tag{A45}$$

$$\delta(y-d)\left(D\left[\frac{\partial^3 \overline{w}_s}{\partial y^3}\right]_{y=d} + (k_d - ic\omega)(\overline{w}_s - \overline{w}_1)\right) = 0, \tag{A46}$$

$$\delta(y-d)\left(D\left[\frac{\partial^3 \overline{w}_s}{\partial y^3}\right]_{y=d} + (k_d - ic\omega)(\overline{w}_s - \overline{w}_1)\right) = 0, \tag{A47}$$

$$\frac{d}{dy}\delta(y\mp d)\left(D\left[\frac{\partial^2 \overline{w}_s}{\partial y^2}\right]_{y=\pm d} - 2Dk_x^2[\overline{w}_s]_{y=\pm d}\right) = 0, \tag{A48}$$

$$\frac{d^2}{dy^2}\delta(y\mp d)\left(D\left[\frac{\partial \overline{w}_s}{\partial y}\right]_{y=\pm d}\right) = 0, \tag{A49}$$

$$\frac{d^3}{dy^3}\delta(y\mp d)\left(D[\overline{w}_s]_{y=\pm d}\right) = 0, \tag{A50}$$

which results in Eqs.(22)-(24).

Appendix B

To study the two-dimensional model numerically, the following parameters of the system have been used:

ρ_r =7800 [kg/m^3]; ρ_s =2500 [kg/m^3]; h =0.612 [m]; d =0.75 [m]; a =1.25 [m];
E_r =2.1 10^{11} [N/m^2]; E_s =31 10^9 [N/m^2]; κ_d =5.25 10^7 [N/m^2]; χ =9.0 10^7 [N/m^3];
c =4980 [Ns/m^2]; P =10^5 [N]; ν =0.3;
A_r =76.9 10^{-4} [m^2] (for one rail $A_{UIC\ 60}$=76.9 10^{-4} [m^2]);
I_r =3055 10^{-8}[m^4] (for one rail $I_{UIC\ 60}$=3055 10^{-8} [m^4]);

ρ_1 =7800 [kg/m^3]; ρ_2 =2500 [kg/m^3]; E_1 =2.1 10^{11} [N/m^2]; E_2 =31 10^9 [N/m^2];
A_1 =153.8 10^{-4} [m^2]; (two rails = $2A_{UIC\ 60}$ = 1.538 10^{-2} [m^2]);
I_1 =6.11 10^{-5} [m^4]; (two rails=$2I_{UIC\ 60}$=6.11 10^{-5} [m^2]);
A_2 =1.53 [m^2]; (concrete strip with the width 2.5 m and the thickness=0.612 m)
I_2 =4775.0 10^{-5} [m^4]; (concrete strip with the width 2.5 m and the thickness=0.612 m)
κ_d =1.05 10^8 [N/m^2]; (two rails=$2k_{\text{fill material}}$=1.05 10^8 [N/m^2]);
χ =2.25 10^8 [N/m^2]; (χ_{subsoil}= 9 10^7 [N/m^3]*2.5=2.25 10^8 [N/m^3]);

c=9960 [Ns/m^2]; (two rails=2$c_{\text{fill material}}$=9960 [Ns/m^2]);
P=2 10^5 [N];

Appendix C

$$[a]=\begin{bmatrix}
\frac{1}{q_1} & \frac{1}{q_2} & q_1 & q_2 & -\frac{1}{q_1} & -\frac{1}{q_2} & -q_1 & -q_2 & 0 & 0 & 0 & 0 \\
0 & 0 & 0 & 0 & q_1 & q_2 & \frac{1}{q_1} & \frac{1}{q_2} & -q_1 & -q_2 & -\frac{1}{q_1} & -\frac{1}{q_2} \\
\frac{\lambda_1}{q_1} & \frac{\lambda_2}{q_2} & -\lambda_1 q_1 & -\lambda_2 q_2 & -\frac{\lambda_1}{q_1} & -\frac{\lambda_2}{q_2} & \lambda_1 q_1 & \lambda_2 q_2 & 0 & 0 & 0 & 0 \\
0 & 0 & 0 & 0 & \lambda_1 q_1 & \lambda_2 q_2 & -\frac{\lambda_1}{q_1} & -\frac{\lambda_2}{q_2} & -\lambda_1 q_1 & -\lambda_2 q_2 & \frac{\lambda_1}{q_1} & \frac{\lambda_2}{q_2} \\
\frac{\lambda_1^2}{q_1} & \frac{\lambda_2^2}{q_2} & \lambda_1^2 q_1 & \lambda_2^2 q_2 & -\frac{\lambda_1^2}{q_1} & -\frac{\lambda_2^2}{q_2} & -\lambda_1^2 q_1 & -\lambda_2^2 q_2 & 0 & 0 & 0 & 0 \\
0 & 0 & 0 & 0 & \lambda_1^2 q_1 & \lambda_2^2 q_2 & \frac{\lambda_1^2}{q_1} & \frac{\lambda_2^2}{q_2} & -\lambda_1^2 q_1 & -\lambda_2^2 q_2 & -\frac{\lambda_1^2}{q_1} & -\frac{\lambda_2^2}{q_2} \\
\frac{C_1}{p_1} & \frac{C_2}{p_2} & C_1 p_1 & C_2 p_2 & 0 & 0 & 0 & 0 & 0 & 0 & 0 & 0 \\
0 & 0 & 0 & 0 & 0 & 0 & 0 & 0 & C_1 p_1 & C_2 p_2 & \frac{C_1}{p_1} & \frac{C_2}{p_2} \\
\frac{C_3}{p_1} & \frac{C_4}{p_2} & -C_3 p_1 & -C_4 p_2 & 0 & 0 & 0 & 0 & 0 & 0 & 0 & 0 \\
0 & 0 & 0 & 0 & 0 & 0 & 0 & 0 & C_3 p_1 & C_4 p_2 & -\frac{C_3}{p_1} & -\frac{C_4}{p_2} \\
-\frac{\lambda_1^3}{q_1} & -\frac{\lambda_2^3}{q_2} & \lambda_1^3 q_1 & \lambda_2^3 q_2 & \frac{C_5}{q_1} & \frac{C_6}{q_2} & C_7 q_1 & C_8 q_2 & 0 & 0 & 0 & 0 \\
0 & 0 & 0 & 0 & C_7 q_1 & C_8 q_2 & \frac{C_5}{q_1} & \frac{C_6}{q_2} & \lambda_1^3 q_1 & \lambda_2^3 q_2 & -\frac{\lambda_1^3}{q_1} & -\frac{\lambda_2^3}{q_2}
\end{bmatrix}$$

$q_1=\exp(\lambda_1 d),\ q_2=\exp(\lambda_2 d),\ p_1=\exp(\lambda_1 a),\ p_2=\exp(\lambda_2 a),$

$C_1=(\lambda_1^2-\nu k_x^2),\ C_2=(\lambda_2^2-\nu k_x^2),\ C_3=\lambda_1(\lambda_1^2+(\nu-2)k_x^2),\ C_4=\lambda_2(\lambda_2^2+(\nu-2)k_x^2)$

$C_5=(\lambda_1^3-S_1),\ C_6=(\lambda_2^3-S_1),\ C_7=-(\lambda_1^3+S_1),\ C_8=-(\lambda_2^3+S_1)$

$$S_1=\frac{k_d(\rho_r A_r\omega^2-E_r I_r k_x^4)}{D(-\rho_r A_r\omega^2+E_r I_r k_x^4+k_d-ic\omega)},\quad S_2=\frac{-2\pi P k_d}{D(-\rho_r A_r\omega^2+E_r I_r k_x^4+k_d-ic\omega)}$$

$$\vec{F}=\begin{bmatrix}0 & 0 & 0 & 0 & 0 & 0 & 0 & 0 & 0 & S_2 & S_2\exp(i\varphi)\end{bmatrix}$$

References

- [1] Filippov, A.P.: Steady state vibrations of an infinite beam on an elastic half-space subjected to a moving load (in Russian). Izvestija Akademii Nauk SSSR Mehanika I Mashinostroenie 6

(1961) 97-105
- [2] Labra, J. J.: An axially stressed railroad track on an elastic continuum subjected to a moving load. Acta Mechanica 22, (1975) 113-129
- [3] Krylov, V.V.: Generation of ground vibrations by superfast trains, Applied Acoustics 44/2 (1995) 149-164
- [4] Dieterman, H. A.; Metrikine, A. V.: Steady-state displacements of a beam on an elastic half-space due to a uniformly moving constant load. Eur J Mech A/Solids 16/2 (1997) 295-306
- [5] Suiker, A.S.J.; de Borst, R.; Esveld, C.: Critical behaviour of a Timoshenko beam-half plane system under a moving load. Arch Appl Mech 68 (1998) 158-168
- [6] Grundmann, H.; Lieb, M.; Trommer, E.: The response of a layered half-space to traffic loads moving along its surface. Arch Appl Mech 69/1 (1999) 55-67
- [7] Sheng, X., Jones, C.J.C., Petyt, M.: Ground vibration generated by a load moving along a railway track. J Sound Vibr 228/1 (1999) 129-156
- [8] Metrikine, A.V.; Popp, K.: Vibration of a periodically supported beam on an elastic half-space. Eur J Mech A/Solids 18/4 (1999) 679-701
- [9] Kaynia, A.M.; Madhus, C.; Zackrisson, P.: Ground vibration from high-speed trains: prediction and countermeasure. J Geotech Geoenvironm Eng 126/6 (2000) 531-537
- [10] Kononov, A.V.; Wolfert, A.R.M.: Load motion along a beam on a viscoelastic half-space. Eur J Mech A/Solids 19 (2000) 361-371.
- [11] Lombaert, G; Degrande, G; Clouteau, D.: Numerical modelling of free field traffic vibrations. Soil Dyn Earthq Eng 19/7 (2000) 473-488
- [12] Vestnitskii, A.I.; Metrikine A.V.: Transition radiation in mechanics. Physics Uspehi 39 (1996) 983-1007
- [13] Fryba, L.: Vibration of solids and structures under moving loads. London: Telford 1999
- [14] Achenbach J.D.: Wave propagation in elastic solids. North-Holland Publishing Company: Amsterdam-London 1973.
- [15] Kononov, A.V.; Dieterman, H. A.: A uniformly moving constant load along a Winkler supported strip. Eur J Mech A/Solids 18 (1999) 731-743
- [16] Vladimirov, V.S.: Equations of Mathematical Physics. Marcel Dekker: New York 1971
- [17] Vesnitskii, A.I.: Waves in systems with moving borders and loads (in Russian). Moscow: Nauka 2001
- [18] Dieterman, H.A.; Metrikine, A.V.: Critical velocities of a harmonic load moving uniformly along an elastic layer, Trans ASME J Appl Mech 64 (1997) 596-600
- [19] Metrikine, A.V.; Vrouwenvelder, A.C.W.M.: Surface ground vibration due to a moving train in a tunnel: two-dimensional model,", J Sound Vibr 234/1 (2000) 43-66
- [20] Bogacz, R.; Krzyzynski, T.; Popp, K.: On the Generalization of Mathews' Problem of the Vibrations of a Beam on Elastic Foundation. ZAMM 69 (1989) 243-252
- [21] Dieterman, H. A.; Metrikine, A. V.: The equivalent stiffness of a half-space interacting with a beam. Critical velocities of a moving load along the beam. Eur J Mech A/Solids 15/1 (1996) 67-90